Manuscript prepared for Ocean Sci. Discuss.
with version 2015/04/24 7.83 Copernicus papers of the LaTeX class copernicus.cls.
Date: 17 March 2016

Compensation between meridional flow components of the AMOC at 26° N

E. Frajka-Williams[1], C. S. Meinen[2], W. E. Johns[3], D. A. Smeed[4], A. Duchez[4], A. J. Lawrence[1], D. A. Cuthbertson[1], G. D. McCarthy[4], H. L. Bryden[1], M. O. Baringer[2], B. I. Moat[4], and D. Rayner[4]

[1]Ocean and Earth Science, University of Southampton, National Oceanography Centre Southampton, SO14 3ZH, UK
[2]Atlantic Oceanographic and Meteorological Laboratory, Physical Oceanography Division, 4301 Rickenbacker Causeway, Miami, FL 33149, USA
[3]University of Miami, Rosentiel School of Marine and Atmospheric Science, 4600 Rickenbacker Causeway, Miami, FL, USA
[4]National Oceanography Centre, Waterfront Campus, European Way, Southampton, SO14 3ZH, UK

Correspondence to: E. Frajka-Williams (e.frajka-williams@soton.ac.uk)

Abstract

From ten years of observations of the Atlantic meridional overturning circulation at 26° N (MOC, 2004–2014), we revisit the question of flow compensation between components of the circulation. Contrasting with early results from the observations, transport variations of the Florida Current (FC) and upper mid-ocean transports (UMO, top 1000 m east of the Bahamas) are now found to compensate on sub-annual timescales. The observed compensation between the FC and UMO transports is associated with horizontal circulation and means that this part of the correlated variability does not project onto the MOC. A deep baroclinic response to wind-forcing (Ekman transport) is also found in the lower North Atlantic Deep Water (LNADW, 3000–5000 m) transport. In contrast, covariability between Ekman and the LNADW transports does contribute to overturning. On longer timescales, the southward UMO transport has continued to strengthen, resulting in a continued decline of the MOC. Most of this interannual variability of the MOC can be traced to changes in isopycnal displacements on the western boundary, within the top 1000 m and below 2000 m. Substantial trends are observed in isopycnal displacements in the deep ocean, underscoring the importance of deep boundary measurements to capture the variability of the Atlantic MOC.

1 Introduction

The Atlantic meridional overturning circulation (MOC) is a key part of the global ocean circulation, redistributing heat and properties around the globe. The continuous daily time-series observations at 26° N (Fig. 1) are the first of their kind, capturing the transbasin circulation variability on timescales of days to – now – a decade.

From the first year of observations, Cunningham et al. (2007) noted considerable high-frequency variability of the MOC, with values ranging from 5–35 Sv. This exceeds the range of all previous estimates of the MOC strength at 26° N derived from hydrographic sections (Bryden et al., 2005). After three years of data were recovered, a seasonal cycle of the MOC

became apparent (Kanzow et al., 2010), with a maximum in July–November and a minimum in March, and a seasonal range of approximately $\pm 3.5\,\mathrm{Sv}$. This seasonal cycle has been captured by numerical simulations (Xu et al., 2014) and may be explained by variations in wind-forcing on seasonal timescales (Yang, 2015; Duchez et al., 2014). Kanzow et al. (2010) also noted that the components of the MOC (the Florida Current, the interior thermal-wind contribution and the Ekman flow) were largely uncorrelated, suggesting that each contributes variability to the MOC independently. Once the MOC records had stretched to seven years in length, striking interannual variability and more recently a declining trend in the MOC were revealed (McCarthy et al., 2012; Smeed et al., 2014). These low frequency transport changes have been shown to be responsible for changes in ocean heat content in the subtropical and tropical North Atlantic (Cunningham et al., 2014; Bryden et al., 2014).

Numerical investigations into the sources of variability to the Atlantic MOC interannual variability suggest that much of the variability may be attributable to winds (Cabanes et al., 2008; Roberts et al., 2013; Zhao and Johns, 2014; Yang, 2015; Pillar et al., 2016). Buoyancy forcing instead affects decadal variations (Polo et al., 2014; Yeager, 2015). An estimate of the MOC from high latitude density anomalies suggests a decline of the MOC (Robson et al., 2014) which is presently observed at 26° N (observed trend of $-0.5\,\mathrm{Sv/yr}$, Smeed et al., 2014) though it may not be indicative of a longer-term decline (Roberts et al., 2014). The 26° N array provides an estimate of the MOC, but separating it into components and even depth ranges of anomalies may aid in the identification of physical causes of change (Wunsch and Heimbach, 2013).

In this paper, we introduce the 10 year record of the MOC at 26° N, describing features of the variability in the most recent 18 months and across the ten-year record, and examine more fully the degree of correlation or compensation between MOC components using the longer records. While much of the recent research into Atlantic MOC variability has focused on interannual timescales and longer, here we quantify newly observed compensation between the Florida Current and UMO transports, and covariability between the deep transbasin transports and zonal winds, on sub-annual timescales. The depth structure and time scales of these variations are explored, illustrating an important role for the western

boundary below 1000 m. Lower frequency changes in MOC components, including the continuing trend in the vertical shear of the mid-ocean transport, are also described. Finally, we conclude by discussing the origins of the lower-frequency variability in the 10 year records.

2 Methods

The international 26° N RAPID Climate Change/Meridional overturning circulation and heat flux array (hereafter RAPID 26° N) has provided comprehensive daily measurements of the MOC at 26° N for ten years so far (April 2004–March 2014; Smeed et al., 2015). The MOC is defined as the northward transport above the depth of maximum overturning (roughly 1100 m) across 26° N, and is constructed as the sum of three components: the surface meridional Ekman transport (Ek) estimated from reanalysis winds, the Gulf Stream transport through the Florida Straits – the Florida Current (FC) – measured by a submarine cable (e.g. Meinen et al., 2010), and the upper mid-ocean (UMO) transport, measured by a trans-basin array of current meter and dynamic height moorings between the Bahamas and Africa. The exact number of moorings and instruments has varied over the past decade during which there have been over 20 deployment and recovery cruises. The main western boundary mooring which we used here is called WB2, and typically has 18 MicroCAT (Seabird Electronics, Bellevue, WA) conductivity–temperature–depth instruments. Vertical resolution ranges from 75 m near the surface to 500 m near the bottom. Overall, the accuracy of the MOC transport is estimated to be 1.5 Sv (ten-day values) or 0.9 Sv (annual averages). Full details of the array configuration and map (their figure 1.1),, transport calculation and associated errors can be found in McCarthy et al. (2015).

Here, we focus on the trans-basin or mid-ocean (MO) transport, from which the UMO is derived. The MO transport is constructed from three parts:

$$\mathrm{MO}(z) = T_{\mathrm{wbw}}(z) + T_{\mathrm{int}}(z) + T_{\mathrm{ext}}(z), \tag{1}$$

where T_{wbw} is the western boundary transport estimated from direct current meter measurements, T_{int} the "internal" transbasin transport and T_{ext} the "external" flow. The west-

ern boundary wedge transport, T_{wbw} includes most of the flow associated with the Antilles Current. The "internal" transport, T_{int}, is the baroclinic flow zonally-integrated across the remainder of the ocean interior relative to an assumed level of no motion at 4820 dbar. It is derived from dynamic height moorings near the western and eastern boundaries and over the Mid-Atlantic Ridge (Fig. 1). Here we focus on the western and eastern profile contributions to the T_{int}. Using only the western and eastern density contributions to interior transport-per-unit depth, we have that $T_{\text{int}}(z)$ relative to the reference level (z_{ref}) is related to density as

$$T_{\text{int}}(z) = -\frac{g}{f\rho}\int_{z_{\text{ref}}}^{z} \left[\rho_{\text{e}}(z') - \rho_{\text{w}}(z')\right] \mathrm{d}z', \tag{2}$$

where g is gravitational acceleration, f the Coriolis parameter, and $\rho_{\text{e}}(z)$ and $\rho_{\text{w}}(z)$ the density profiles at the eastern and western boundary, respectively (Rayner et al., 2011).

The "external" flow, T_{ext}, is the (unmeasured) interior barotropic flow that ensures zero mass transport across the section. This component is calculated as a residual of the other components and is applied as a uniformly-distributed, and thus depth-independent, velocity across the entire mid-ocean section, which we refer to as "hypsometric compensation". Due to changes in the width of the basin as a function of depth, even though the applied flow is barotropic, the transport-per-unit-depth has decreasing magnitude with increasing depth. Kanzow et al. (2007) showed that this estimate – derived from mass conservation – was in good agreement with an independent estimate of the mid-ocean barotropic flow derived from bottom pressure gauges deployed across the section over the April 2004-April 2005 period.

The MO transport can be further divided into its contributions to the upper and lower branches of the overturning circulation. The UMO is defined as the depth-integral of MO transport between the surface and the time-varying depth of maximum overturning, roughly 1100 m. The lower limb of the MOC is made up of southward flowing North Atlantic Deep Water, which is split into contributions associated with upper North Atlantic Deep Water

(UNADW; 1100–3000 m) and lower North Atlantic Deep Water (LNADW; 3000–5000 m). The sum of these two transports recovers nearly all the variability of the MOC ($r = 0.996$, McCarthy et al., 2012). The small difference is equal to the flow between 1100 m and the depth of maximum overturning and a contribution from the hypsometric compensation below 4820 bar.

For the analysis presented here, we start with the RAPID data as processed for the publicly available dataset. This processing involves filtering individual instrument records with a two-day low-pass filter to remove the tides, and subsampling onto 12-hourly intervals. From this subsampled dataset, transport components are computed, then further ten-day low-pass filtered with a 5-th order Butterworth filter before the compensation transport is calculated (Kanzow et al., 2007). These data are available from http://rapid.ac.uk. Here we additionally bin the data onto a twice-monthly time grid, then remove the twice-monthly climatology to reduce seasonal variations. For lower frequency variations, deseasonalized time series are further filtered with a 1.5 year Tukey filter. Significance and confidence intervals are reported at the 95 % level, unless otherwise indicated. The number of degrees of freedom was calculated using the integral timescale of decorrelation to the first zero crossing (Emery and Thomson, 2004). When a year is denoted 2009/10, it refers to the period 1 April 2009 through 31 March 2010.

For the purpose of calculating isopycnal displacements ζ, absolute salinities and conservative temperatures on the twice-monthly time grid are used. Isopycnal (σ) displacements are then calculated following Desaubies and Gregg (1981), as

$$\zeta(\bar{z}(\sigma_i), t) = z(\sigma_i, t) - \bar{z}(\sigma_i) \ ,$$

using locally-referenced densities. For example, to determine the displacement of the isopycnal typically found at 1000 dbar, potential densities are calculated referenced to 1000 dbar (σ_1). Using these locally-referenced densities, the mean density at 1000 dbar is identified ($\sigma_i = \langle \sigma_1(z = 1000, t) \rangle_t$). The depth of this density, $z(\sigma_i, t)$, is then determined for each timestep in the locally-referenced densities, and differenced from its mean depth (~991 m for 1000 dbar). This produces isopycnal displacements as a function of density, which can

then be mapped back onto depth using the mean relationship between depth and density ($\bar{z}(\sigma_i)$). This process of locally-referencing densities is repeated for each pressure surface from the surface to the bottom at 20 dbar intervals.

For reference pressures from the surface to bottom, a mean density profile is calculated within 400 m of the reference pressure, and isopycnal displacements from the mean depth are calculated. Displacements are then mapped back onto the mean depth of each density surface using the time mean profile. The detrended and low-pass filtered time series are processed as above.

3 Ten years of MOC and mid-ocean variability

All of the ten-year time series of transport components at 26° N show high frequency variability (Fig. 2a). In the most recent 18 months, additional features of the time series include a large Ekman transport reversal in March 2013 (similar to the two reversals that occurred in 2009/10 and 2010/11). During the March 2013 event, the Ekman transport anomalies exceeded two standard deviations from the mean, with the typically northward-flowing water turned to the south. This reversal was similar in magnitude to the December 2009–March 2010 event, but with shorter duration (Fig. 2a). On several occasions, as during the negative Ekman events in 2005, 2010 and 2013, the FC also showed sharp, short-term reductions in transport. These corresponding anomalies led to sharp reductions – or even brief reversals – of the MOC at these times. Over the past 10 years, the MOC was negative from 19-24 December 2009, and from 9-13 March 2013. The Ekman transport reversals also coincided with reductions of the southward LNADW flow (Fig. 2b). In the most recent 5 years, the LNADW experienced more short periods of reversal (i.e., a northward flow of the net transport below 3000 m) than had been observed in the first 5 years of the record. These high frequency events in the deep flow exhibit fairly weak vertical shear, with maximum anomalies below 3000 m (Fig. 3a).

The MOC exhibits substantial variability at time scales longer than annual (Fig. 4). Interannual variability of the MOC derives primarily from the UMO component, with a negative

trend in both over the full 10 year record. The mean and standard deviation of the MOC for the first five years of observations is 18.4 ± 1.3 Sv and the second five years 15.5 ± 1.9 Sv (these values are significantly different, see Table 1). While some of this change is contributed by the 2009/10 dip (McCarthy et al., 2012), the intensification of the southward thermocline flow (UMO) has persisted with the associated weakening of the MOC. The 2012/13 year was the second weakest year of the MOC (14.2 Sv), behind the 2009/10 year (12.8 Sv). In contrast to the 2009/10 year, the weak MOC in 2012/13 had very little contribution from the wind-driven Ekman transport, but instead is associated with a strong southward thermocline flow (UMO).

Transport-per-unit depth anomaly profiles show the depth-structure of mid-ocean transport variations. In the top 1100 m, the southward UMO has intensified (Fig. 3b, shift from red to blue), while below 3000 m the southward LNADW has weakened (shift from blue to red). Previous analyses have shown that variability of the UMO on interannual timescales is primarily governed by changes at the western boundary (Frajka-Williams, 2015). The amplitude of these changes is larger in the top 1000 m, but anomalies below 1000 m span a large portion of the water column.

4 Correlation between transport components

During the first three years of observations (2004–2007), the components of the MOC (FC, UMO and Ekman) showed little covariability, leading to the conclusion that components contribute their variability independently to the MOC (Kanzow et al., 2010). More recently, sporadic periods of covariability were identified between currents at the western boundary: the FC and Antilles Current from 2009 to 2011 (the end of the record at the time of publication) (Frajka-Williams et al., 2013). From the ten-year record (2004–2014), we now see correlations emerging between some of the contributing terms, which has implications for how we understand the large-scale circulation at 26° N. Considering the 3 month filtered UMO and FC transport time series (black lines in Fig. 2), anomalies of opposite sign appear to coincide in late 2008, late 2010 and again in late 2012. During the 2010/11 winter, for

example, the northward flowing FC weakened by several Sverdrups. At the same time, the southward flowing UMO weakened by nearly 10 Sv. We investigate these apparent compensations (between the UMO and FC, and also between LNADW and wind-driven Ekman flow) more rigorously in the following section.

4.1 UMO and FC transports: Horizontal circulation

The FC carries most of the waters of the Gulf Stream across 26° N. The origins of this water come from the Yucatan Channel and Old Bahama Channel, across complex topography west of the Bahamas (Rousset and Beal, 2014). At similar latitudes, the flow through the Yucatan Channel has been found to compensate flow around Cuba (Lin et al., 2009), while variations in the FC have, at times, shown compensation east of the Bahamas in bottom pressure variations (Bryden et al., 2009) and in top 1000 m velocities (Frajka-Williams et al., 2013).

Here we consider compensation between FC and UMO, the transbasin transport east of the Bahamas. This compensation can be clearly seen by plotting their detrended anomaly time series (Fig. 5a). Certain events stand out, demonstrating almost perfect correspondence between the two time series, with examples including February–May 2007, September 2008–June 2009, August 2010–January 2011 and August 2012–March 2013 (highlighted in the figure). Notably, these episodes of correlation are absent in the first 3 years. The overall correlation between the two records is $r = -0.49$, significant at the 95 % level.

Fluctuations in UMO compensate fluctuations in the FC by similar magnitudes (slope $= -0.92$, Fig. 5b). When the northward FC transport increases along the western boundary, the southward UMO transport east of the Bahamas intensifies by the same amount. This means that excess northward flow in the boundary current is returned horizontally within the upper mid-ocean circulation rather than by deeper layers in the interior, which would have involved changes in the MOC. The region east of the Bahamas is known to be rich with eddies which may influence the transbasin transports (Wunsch, 2008; Kanzow et al., 2009; Thomas and Zhai, 2013; Clément et al., 2014; Xu et al., 2014), and due to the timescale of observed compensation, we suspect that eddies are involved.

Using the low-pass filtered time series, this high degree of compensation is absent (Fig. 5c and d). Instead, strong interannual variability in the UMO remains (Fig. 5c). By comparison, the low-pass filtered FC shows little interannual variability, consistent with previous work that indicated that the interannual and longer period FC variability is of much smaller amplitude than the sub-annual variability (e.g. DiNezio et al., 2009; Meinen et al., 2010). While the two time series are not significantly correlated ($r = 0.24$), both show a reduction from the first five-year period (April 2004–March 2009) to the latter five-year period (April 2009–March 2014, see also Table 1), with the FC reducing by 0.7 Sv and the UMO by 1.9 Sv. Unlike the compensation at higher frequencies, these changes are both of the same sign (note that the negative of UMO is plotted in Fig. 5a), compounding the effect on the MOC (net reduction of 2.9 Sv).

4.2 LNADW and Ekman transports: Deep wind-driven response

Another – and perhaps more remarkable – correlation that emerges from this analysis is between the deepest limb of the southward mid-ocean transports (LNADW) and the surface meridional Ekman transport (Fig. 6a). Using the detrended anomaly time series, the typically southward LNADW transport can be seen to reduce or even temporarily reverse to northward during strong Ekman transport reversals. (See e.g., events in December 2009–April 2010, November 2010–January 2011, February–March 2013.) The correlation is statistically significant ($r = -0.58$), and can be seen to occur throughout much of the record rather than just during the extreme events. In the low-pass filtered data (Fig. 6c and d), the correlation is stronger than for the UMO and FC. However, due to the low number of degrees of freedom for the low-pass filtered time series (ndof $= 5$), it is not significant.

As with the FC and UMO compensation, magnitudes of fluctuations between Ekman and LNADW match (slope $= -0.84$, with Ekman anomalies of 1 Sv corresponding to a 0.84 Sv change in the LNADW). Unlike for the FC and UMO, however, the correlation between the LNADW and Ekman at higher frequencies projects onto the MOC rather than cancelling. This is consistent with expectations that the high frequency, wind-driven variability of Ekman transport results in an overturning, albeit a shallow one (where the depth of overturning is

at the base of the northward Ekman transport) between the surface Ekman transport and return flow below (Jayne and Marotzke, 2001; Killworth, 2008). Variations in Ekman or FC project directly on the mid-ocean transport (through the T_{ext} term in 2), and bottom pressure records at the western boundary also covary with Ekman anomalies (McCarthy et al., 2012). However, we will show that the covariations between FC, Ekman and mid-ocean transports are not limited to the T_{ext} contribution, but are instead associated with density changes at the western boundary.

To identify possible lags between the UMO and FC or Ekman and LNADW, we use the 10 day filtered time series. For both correlations, between the UMO and FC and between the Ekman and LNADW, the timescale of the response is fast (Fig. 7). For the LNADW and Ekman correlation, a maximum correlation of $r = 0.51$ is found at 1 day lag with Ekman leading. This means that the wind response occurs essentially instantaneously. For the UMO and FC transports, a maximum correlation of $r = 0.46$ is found for UMO leading by 0.5 days. This lead-lag relationship can also be seen by inspecting close-zoomed plots of the time series during large anomalies (Fig. 7e). Due to filtering applied to individual instrument data and transport time series, such a short lag is not statistically meaningful.

5 Depth structure of covariability

The hypsometric compensation term (T_{ext}) is mostly depth-independent, but has a vertical profile that scales with the width of the basin as a function of depth. It is nearly uniform from the surface to about 3500 m, and then decreases gradually to zero at the greatest depths in the basin. If the mid-ocean region had no shear (T_{int}=0) and no flow in the wedge ($T_{\text{wbw}} = 0$), the MO transport would still be non-zero through this applied compensation, in order to balance the northward FC and Ekman transport. In the absence of strong variations in T_{int}, we would expect to see anti-correlation between the MO transports (e.g., the UMO and LNADW) and the independently estimated FC and Ekman transports. In this case, the MO transport fluctuations would then have a depth structure approximately matching

the hypsometric profile. Instead, the MO transport-per-unit-depth profiles often show deep maxima below 3500 m in anomaly plots (Fig. 3a).

The deep maximum in transport-per-unit-depth implies that there are considerable changes in the deep shear integrated across the width of the basin, which are reflected in the T_{int} term. (There is little transport in the T_{wbw} term below 2000m.) The T_{int} term, in turn, is determined by the isopycnal displacements at the eastern and western boundaries, according to a basin-wide thermal wind balance. In the following, we will use isopycnal displacements at the two basin boundaries to investigate the vertical structure of the variability noted above. In the simplest case of a two-layer fluid, a tilted interface marked by the displacement of the interface at the boundaries will have an associated geostrophic shear between the layers. The strength of the shear increases with the tilt of the interface so that if the interface were at a constant depth at the eastern boundary, the shear would be controlled by displacements at the western boundary.

While the stratification at 26° N is more continuous, we use displacements at the two basin boundaries to investigate the magnitude of the shear variability and the role of east and west in producing these shear anomalies. Using the time-mean density gradient profile, given by $\overline{N}^2(z) = -(g/\rho)\partial\bar{\rho}/\partial z$, the contribution of heave to transport-per-unit-depth can be estimated from Eq. (2) as

$$\widetilde{T}_{\text{int}}(z) = \frac{1}{f}\int_{z_{\text{zref}}}^{z} \zeta_{\text{e}}\overline{N_{\text{e}}}^2 - \zeta_{\text{w}}\overline{N_{\text{w}}}^2 \,\mathrm{d}z', \tag{3}$$

where $\sim$ distinguishes this portion of T_{int} from the more complete calculation in (2). Here, $\zeta_{\text{e}}(z,t)$ and $\zeta_{\text{w}}(z,t)$ are the isopycnal displacements at the east and west, respectively. From (3), we might expect some correspondence between isopycnal displacements and transports, though transports are the vertically-integrated transport-per-unit-depth.

Comparing the UMO transport with both eastern and western boundary isopycnal displacement time series, we find strong correlations (Fig. 8a). In the west, displacements between 300 and 1200 m are significantly correlated with the UMO time series, with a peak

at 820 m. This is consistent with physical expectations, and prior results indicated a role for the displacement of the main thermocline in controlling the UMO transport (Longworth et al., 2011; McCarthy et al., 2012; Duchez et al., 2014). The correlation in the east is of similar absolute amplitude but is spread over a broader depth range (200 to $\sim$ 1800 m deep), consistent with the findings of Chidichimo et al. (2010) that the eastern boundary density variations were coherent down to 1400 m. No significant correlations were found between any of the transport components considered here (UMO, FC, LNADW or Ekman) and the isopycnal displacements at the Mid-Atlantic ridge (not shown).

The FC is also highly correlated with the western boundary thermocline displacement (Fig. 8a). The sign of the correlation has flipped, consistent with the anti-correlation noted between the FC and UMO. This relationship is statistically significant, even though the isotherms covarying with the FC are 150 km away from the FC, east of the Bahamas. As might be expected, there is no statistically significant relationship between the thermocline displacements on the eastern side of the basin and the FC transport. Comparing the time series of western boundary isopycnal displacements at 820 m with the UMO transport (Fig. 9a), we find significant correlation where a 10 m downward displacement of the thermocline corresponds to a 1 Sv increase in the UMO transport (Fig. 9b). Given the one-to-one relationship between the FC and UMO (Fig. 5b), this means that a 10 m thermocline displacement is also associated with a 1 Sv change in the FC.

The correlation between LNADW transport and isopycnal displacements is significant at depth (1500 m–bottom) on the western boundary only (Fig. 8b). The negative correlation can be readily understood in that a depression of deep isopycnals on the western side of the basin causes larger northward shear below 2000 m. That is to say, a depression of deep isopycnals on the western side of the basin will result in a slowing of the southward LNADW (a northward anomaly) relative to the UNADW layer above it. One remarkable feature of this correlation is that it extends vertically over several thousand meters of water (spanning several moored instruments), so that when water at 3000 m moves upwards, a large segment of the water column above and below is also moving upwards (though

with differing magnitudes). In this case, a 42 m downward displacement of the isopycnal at 3140 m results in a 1 Sv reduction in the LNADW transport (Fig. 9d).

Isopycnal displacements in a reduced region (2700–3300 m) at the western boundary are also significantly correlated with the surface Ekman transport (Fig. 8b). Positive (northward) Ekman transport anomalies are associated with upward displacements of the deep isopycnals. This means that when the winds blow along 26° N, the deep ocean responds by heaving upwards or downwards across hundreds of meters, with the end result that these isopycnal displacements at the western boundary change the basin-wide tilt and thus the vertical shear in meridional transports. Just 40 km offshore (25 km further offshore than the western boundary) at the WB3 mooring, isopycnal displacements are still significantly correlated with LNADW transports, albeit more weakly ($|r| \leq 0.5$, not shown). Ekman transports are no longer correlated with displacements. At the WB5 mooring, 500 km offshore, there is no relationship between isopycnal displacements and basinwide transport. The strong correlation between isopycnal displacements nearshore and meridional Ekman transport, and the absence of correlation for offshore displacements may indicate that the deep compensation is concentrated at the western boundary, or that other variability in isopycnal displacements masks the signal offshore.

6 Timescales of compensation/covariability

One of the key results presented here is that the UMO and FC transports often compensate each other – i.e. their signs differ but anomalies match – resulting in greatly reduced impact of their individual fluctuations on the total MOC variability. However, this compensation is dependent on timescales. At low-frequencies, the compensation does not dominate (Fig. 5c), and the large interannual variability and trend in the UMO transport has a strong projection onto the interannual variability and trend of the MOC.

To investigate the covariability for different timescales, we evaluate the coherence calculated using a multitaper spectrum following Percival and Walden (1998) (Fig. 10). The FC and UMO are significantly coherent and out-of-phase (i.e., anti-correlated) at periods less

than 1 year. For periods longer than about a year they are no longer coherent. For Ekman and LNADW transports, they are coherent at periods shorter than 900 days (except near 120 days) and also (nearly) out-of-phase. By contrast, there is little coherence between the Ekman and FC time series (Fig. 10, grey).

These results at first appear to contradict Kanzow et al. (2010), who noted from the first 3 years of observations (2004–2007) that there was no compensation between the FC and UMO. Using a cross-wavelet transform (Grinsted et al., 2004), we can examine the temporal shifts in covariability between MOC components (Fig. 11). Since the beginning of 2008, the FC and UMO covary at annual to sub-annual timescales (consistent with the coherence calculation). Prior to 2008 there is no significant covariation between them (Fig. 11a), consistent with the findings of Kanzow et al. (2010). The cross-wavelet transform of LNADW and Ekman shows that the periods of higher co-variability occur in the latter half of the 10 year record (Fig. 11b). There also exists some power at annual timescales and higher frequencies (e.g., during the wind-reversal events in 2005, 2009/10 and 2013).

The compensation between the FC and UMO is non-stationary. A windowed correlation between the FC and UMO prior to 2007 shows no significant correlation, either between the full time series or the high-pass filtered time series (not shown). From Frajka-Williams et al. (2013), the FC and Antilles Current (AC) were correlated between 2009 and 2011. The AC is a narrow, northward boundary current east of the Bahamas. Its transport is measured by direct current meter measurements in the RAPID array, and is included in the UMO transport. The mean transport of the AC is relatively small (3.6 Sv, compared to 31 Sv in the FC), so that the UMO transport is still net southward. However, since the AC is part of the UMO transport, a correlation between the FC and AC should weaken an anti-correlation between the FC and UMO. The isopycnal displacements associated with UMO and FC variability (Fig. 8) also influence transport in the AC, as long as the AC is geostrophic. The mooring used to estimate isopycnal displacements is at the western edge of the UMO transport, but is east of the core of the northward AC velocities. This means that a downward displacement of isopycnals is associated with an increase in the tilt of the thermocline between Africa and the mooring, but will have an opposing effect on geostrophic transports west

of the mooring, in the Antilles Current. Frajka-Williams et al. (2013) identify stronger eddy activity east of the Bahamas during the period of FC and AC correlation, which is consistent with a eddy activity playing a role in the anti-correlation between the FC and UMO on subannual timescales.

7 Trends in isopycnal displacements and MO transports

The MOC at 26° N has been decreasing in strength, as described in Smeed et al. (2014) and this trend continues through early 2014. This low frequency change is mainly associated with uncompensated changes in the UMO transport (variations at timescales longer than 1 year) and to a lesser degree with a weak reduction in the FC transport (Table 1). From the low-pass filtered transport-per-unit depth profiles (Fig. 3b) we noted that changes are present both above and below the thermocline. Here we investigate how the trends in transport are captured by trends in isopycnal displacements.

In the top 1000 m, the isopycnal slope is large, with lighter water in the west. The slope decreases to 0 at about 1000 m, reversing sign between 1000–1500 m, and is typically small below (Fig. 12a). At the western boundary, isopycnal displacements below 1000 m are moving downwards (trend at 3140 m is $-6.5\pm3.5\,\mathrm{m\,yr^{-1}}$, increasing to about $-13\pm0.4\,\mathrm{m\,yr^{-1}}$ at 4500 m), while above 500 m they are moving upwards (Fig. 12b). At the eastern boundary, trends are near zero except below 4000 m where they are downward. As a result, the east-west slope of isopycnals below 1000 m is decreasing with time. While the largest displacements are seen at depth, stratification is also weaker at depth. From Eq. (3), we see that the effect of isopycnal displacements on transports is modulated by the background stratification. Computing instead the trends in isopycnal displacements scaled by stratification (Fig. 12c), we now see that at the western boundary, the effect of isopycnal displacements below the thermocline is nearly constant, with little effect on the eastern boundary. Scaling by stratification emphasizes the importance of relatively small trends in displacements in the top 1000 m to transport anomalies.

The trend in $\widetilde{T}_{\text{int}}$ from Eq. (3) is shown in Fig. 12d, with a persistent reducing trend in the interior transports associated with heave at the eastern and western boundaries. The magnitude of the trend increases from 0 at the bottom, since it is integrated upwards from the bottom. While the thermocline displacement shows little-to-no trend (Fig. 12b, the trend on the western boundary at 830 m is $-0.7 \pm 0.9\,\text{m yr}^{-1}$), the interior transport has a large negative trend. The large amplitude at the depth of the thermocline results from the accumulation of persistent negative anomalies between the bottom and the thermocline. Above 1000 m, the trend in $\widetilde{T}_{\text{int}}(z)$ is relatively constant and negative.

An southward intensification of T_{int}, if unbalanced by other components, would result in an overall intensification of the southward flow across the section over the 10 year period. To maintain overall mass balance across the section, an opposing trend is required in T_{ext} (Fig. 12e). Trends in the overall mid-ocean transport (MO(z)) include those from $\widetilde{T}_{\text{int}}$ as well as anomalies in the wedge and compensation, due to stratification changes and diabatic changes, and both at the boundaries and mid-Atlantic ridge. The overall amplitude of the trend in MO(z) is weaker than in $\widetilde{T}_{\text{int}}(z)$, but with a greater shear near the surface. The wedge in particular contributes to the shear in the top 1000 m in MO(z) relative to $\widetilde{T}_{\text{int}}$ (not shown).

The trend in MO(z) is negative above ~ 1700 m and positive below. This amounts to a rebalancing of the absolute reference level for T_{int} to account for the changing structure of the interior ocean shear profile. Summing the T_{int} and T_{ext} components results in a northward anomaly below 1700 m (where T_{ext} exceeds anomalies in T_{int}). The vertical structure of these trends is consistent with the intensification of the baroclinic circulation: the LNADW is reducing in intensity (less southward than before) while the UMO is increasing in southward flow. In addition, the depth of the change in the trend (1700 m) is in the middle of the UNADW layer (1100–3000 m) offering an explanation for why no long term trend is apparent in the UNADW transport.

8 Discussion

Here we have identified significant compensation, dependent on timescale, between components of the MOC: for example, on sub-annual timescales when the FC is stronger northward in the western boundary, the UMO compensates with stronger southward flow between the Bahamas and Canary islands. While these components are largely independent, they are weakly coupled due to the construction of the MO(z) transports. The T_{ext} term contributes variability to both the UMO and LNADW transport, and would tend to cause an opposite sign anomaly in both the UMO and LNADW in response to anomalies in the FC and Ekman transports.

However, by construction the T_{ext} term is nearly barotropic, and what limited vertical structure it has arises from the vertical profile of section width at 26° N. This means that T_{ext} distributes compensation for the Ekman or FC anomalies across the full water column, with the strongest compensation in the MO(z) term occurring in the top 3500 m and reducing to zero at the bottom. Only a fraction of FC anomalies (order one fifth) would be projected by T_{ext} onto UMO anomalies, and less than half the magnitude of Ekman anomalies would be contained in the LNADW portion of the T_{ext}. Instead, the observed transport anomalies in UMO and LNADW are indistinguishable in magnitude to the anomalies in FC and Ekman transports. Furthermore, there is no correlation between the Ekman and UNADW transport, which requires a shear between LNADW and UNADW to remove any projected compensation to Ekman. We can see this baroclinic response in the isopycnal displacements measured at the western boundary.

The compensation between the UMO and FC has the appearance of a time-varying horizontal or gyre circulation, but is limited to sub-annual timescales similar to those of eddies identified in Frajka-Williams et al. (2013). In that paper, on some occasions, when a large cyclone (anticyclone) impacted the Bahamas (and T_{wbw} transports), the FC would respond by weakening (strengthening). Sea surface height anomalies originating east of the Bahamas coincided with same sign anomalies along the eastern side of the Florida Straits, resulting in transport anomalies of opposite sign to the west and east of the height

anomalies. The new result here is that we use the full UMO rather than just the Antilles Current as in the 2013 paper, and the pattern of anti-correlation has persisted since 2007. Because the co-variability of the FC and UMO transports is accompanied by roughly equal magnitude anomalies, there is a reduced projection of either component on the variability on the overall MOC. This is also consistent with the findings of Clément et al. (2014) who used the RAPID data and sea surface height anomalies to show that Rossby waves/eddies with a sub-annual timescale do contribute to dynamic height anomalies at the boundary but do not affect the MOC.

The relationship between surface winds and deep isopycnal displacements is harder to understand, and we presently do not have a dynamical explanation for this behavior. Nevertheless, the observations are quite clear: when there is anomalous southward Ekman transport (resulting from westerly winds), isopycnals at $\sim 3000\,\mathrm{m}$ on the western boundary plunge downwards. From theoretical and numerical model results (Jayne and Marotzke, 2001; Killworth, 2008), it is expected that Ekman transport fluctuations on sub-annual time scales should result in a quasi-instantaneous, and nearly barotropic, compensation in the deep ocean. One might expect that with anomalous southward Ekman transport across the basin, there should be a northward compensation across a broad range of depths, which could also perhaps be spatially distributed. Yeager (2015) showed in a numerical model that Ekman anomalies project strongly onto the barotropic mode promoting wave interactions with deep bathymetry. It is possible that the baroclinic response we observe at 26° N is generated by these barotropic waves interacting with the bathymetry at the western boundary. This is an area for future research – likely requiring numerical modeling to isolate mechanisms and processes.

The observed high-degree of variability on sub-annual timescales of the UMO and LNADW transports may contribute to the apparent absence of meridional coherence between obsevations at 26° N and higher latitudes. Elipot et al. (2013) found large coherence on short time scales at mid-latitudes in the North Atlantic, but between 41 and 26° N, transport anomalies were out-of-phase (Elipot et al., 2014; Mielke et al., 2013). The large fluctuations in LNADW transport are remarkably well-captured by ocean bottom pressure

from the GRACE satellites (Landerer et al., 2015). However, the spatial footprint of detrended monthly anomalies is centered in the western part of the subtropical North Atlantic, suggesting limited meridional coherence. Using satellite altimetry, Frajka-Williams (2015) found that sea surface height anomalies capture the interannual variability and trend of the UMO transport, with a spatial footprint extending over a larger area.

9 Conclusions

The record of basin-wide MOC transport variability at 26° N in the Atlantic is now ten years long. It continues to deliver new insights into the origins of the changing large-scale circulation at 26° N. In this paper, we have provided a brief overview of the latest 18-months of observations. In particular, with the most recent 18 months of observations, the April 2012 to March 2013 year has the second weakest MOC, behind the 2009/10 year. Unlike the 2009/10 year, the reduction in 2012/13 is associated with an enhanced southward UMO and decreased LNADW, with no contribution from anomalous Ekman transport. There were, however, several wind reversal events in the latest 18 months, at the end of 2012 and again in March 2013. These events were shorter than the 2009/10 and 2010/11 double dip, though they also resulted in concurrent reductions in the southward LNADW transport.

The main result of this paper has been detailing newly-identified compensations between MOC components (UMO and FC, and LNADW and Ekman). Using the ten-year record, we now find that on shorter timescales (periods shorter than 1 year), much of the variability of the UMO is compensated by the FC transport variability, particularly in the most recent seven years. On similar timescales (periods shorter than 2 years), the wind-driven variability in the top 100 m (surface meridional Ekman transport) is nearly instantaneously balanced by deep flow in the opposite direction. However, rather than being a simple barotropic response to the winds, the imprint of the winds is baroclinic, with the strongest signature in isopycnal displacements being found just east of the Bahamas at 3000 m depth.

There is a key difference between these two compensating transport pairs. Between the FC and UMO, compensated high frequency transport anomalies results in a horizontal

circulation anomaly: that is, northward flow in the FC (in the top 700 m) is accompanied by southward flow in the top 1100 m east of the Bahamas. As a consequence, transport anomalies have little influence on the MOC and are unlikely to have a strong heat transport anomaly. By contrast, the southward Ekman anomalies accompanied by northward LNADW anomalies directly projects onto the MOC. During the anomalous periods of exceptionally strong (weak) Ekman transport, the MOC is similarly strong (weak) and we expect the meridional heat transport to vary with the MOC (Johns et al., 2011).

Finally, investigating longer-term variations of the MOC, we can localize the origin of the intensifying trend in the MOC to isopycnal displacements on the western boundary. Observed transport fluctuations on interannual and longer timescales present a different story. From the ten-year record, the mid-ocean transports (rather than FC and Ekman) are primarily responsible for the low frequency variability and trend of the overturning. Furthermore, the trend in transport variability is associated with the persistent deepening of isopycnals below the thermocline at the western boundary. These displacements are greatest in the abyss (130 ± 40 m over 10 years at 4500 m) compared to about 60 ± 30 m at mid-depths around 2000 m, though their impact on transports must be scaled by stratification. While we do not investigate here whether the longer-term isopycnal deepening is associated with watermass changes or wind-forcing, a coincident shift towards warmer and fresher waters below 3000 m (Atkinson et al., 2012) hints at the possibility of larger-scale persistent changes to the Atlantic circulation.

Acknowledgements. Data from the RAPID Climate Change (RAPID)/Meridional overturning circulation and heat flux array (MOCHA), Western Boundary Time Series (WBTS) projects are funded by the Natural Environment Research Council (NERC), National Science Foundation (NSF, OCE1332978) and National Oceanic and Atmospheric Administration (NOAA), the Climate Program Office – Climate Observation Division. Data are freely available from www.rapid.ac.uk.

Florida Current transports are funded by the NOAA and are available from www.aoml.noaa.gov/phod/floridacurrent.

Wavelet code provided by A. Grinsted, J. Moore and S. Jevrejeva. Special thanks to the captains, crews and technicians who have been invaluable in the measurement of the MOC at 26° N over the past ten years.

References

Atkinson, C. P., Bryden, H. L., Cunningham, S. A., and King, B. A.: Atlantic transport variability at 25° N in six hydrographic sections, Ocean Sci., 8, 497–523, doi:10.5194/os-8-497-2012, 2012.

Bryden, H. L., Longworth, H. R., and Cunningham, S. A.: Slowing of the Atlantic meridional overturning circulation at 25° N, Nature, 438, 655–657, 2005.

Bryden, H. L., Mujahid, A., Cunningham, S. A., and Kanzow, T.: Adjustment of the basin-scale circulation at 26° N to variations in Gulf Stream, deep western boundary current and Ekman transports as observed by the Rapid array, Ocean Sci., 5, 421–433, doi:10.5194/os-5-421-2009, 2009.

Bryden, H. L., King, B. A., McCarthy, G. D., and McDonagh, E. L.: Impact of a 30 % reduction in Atlantic meridional overturning during 2009–2010, Ocean Sci., 10, 683–691, doi:10.5194/os-10-683-2014, 2014.

Cabanes, C., Lee, T., and Fu, L.-L.: Mechanisms of interannual variations of the Meridional Overturning Circulation of the North Atlantic, J. Phys. Ocean., 38, 467–480, doi:10.1175/2007JPO3726.1, 2008.

Chidichimo, M. P., Kanzow, T., Cunningham, S. A., Johns, W. E., and Marotzke, J.: The contribution of eastern-boundary density variations to the Atlantic meridional overturning circulation at 26.5° N, Ocean Sci., 6, 475–490, doi:10.5194/os-6-475-2010, 2010.

Clément, L., Frajka-Williams, E., Szuts, Z. B., and Cunningham, S. A.: The vertical structure of eddies and Rossby waves and their effect on the Atlantic MOC at 26° N, J. Geophys. Res., 119, 6479–6498, doi:10.1002/2014JC010146, 2014.

Cunningham, S. A., Kanzow, T., Rayner, D., Baringer, M. O., Johns, W. E., Marotzke, J., Longworth, H. R., Grant, E. M., Hirschi, J. J.-M., Beal, L. M., Meinen, C. S., and Bryden, H. L.: Temporal variability of the Atlantic meridional overturning circulation at 26.5° N, Science, 317, 935–938, 2007.

Cunningham, S. A., Roberts, C., Frajka-Williams, E., Johns, W. E., Hobbs, W., Palmer, M. D., Rayner, D., Smeed, D. A., and McCarthy, G. D.: Atlantic MOC slowdown cooled the subtropical ocean, Geophys. Res. Lett., 40, 6202–6207, doi:10.1002/2013GL058464, 2014.

Desaubies, Y. and Gregg, M. C.: Reversible and irreversible finestructure, J. Phys. Ocean., 11, 541–556, 1981.

DiNezio, P. N., Gramer, L. J., Johns, W. E., Meinen, C. S., and Baringer, M. O.: Observed interannual variability of the Florida Current: Wind forcing and the North Atlantic Oscillation, J. Phys. Oceanogr., 39, 721–736, 2009.

Duchez, A., Frajka-Williams, E., Castro, N., Hirschi, J. J.-M., and Coward, A.: Seasonal to interannual variability in density around the Canary Islands and their influence on the AMOC at 26.5° N, J. Geophys. Res., 119, 1843–1860, doi:10.1002/2013JC009416, 2014.

Elipot, S., Hughes, C., Olhede, S., and Toole, J.: Coherence of western boundary pressure at the RAPID WAVE array: Boundary wave adjustments or deep western boundary current advection?, J. Phys. Oceanogr., 43, 744–765, 2013.

Elipot, S., Frajka-Williams, E., Hughes, C., and Willis, J.: The observed North Atlantic MOC, its meridional coherence and ocean bottom pressure, J. Phys. Oceanogr., 44, 517–537, doi:10.1175/JPO-D-13-026.1, 2014.

Emery, W. J. and Thomson, R. E.: Data Analysis Methods in Physical Oceanography, Elsevier, Amsterdam, the Netherlands, 2nd edn., 2004.

Frajka-Williams, E.: Estimating the Atlantic MOC at 26° N using satellite altimetry and cable measurements, Geophys. Res. Lett., 42, 3458–3464, doi:10.1002/2015GL063220, 2015.

Frajka-Williams, E., Johns, W. E., Meinen, C. S., Beal, L. M., and Cunningham, S. A.: Eddy impacts on the Florida Current, Geophys. Res. Lett., 40, 349–353, doi:10.1002/grl.50115, 2013.

Grinsted, A., Moore, J. C., and Jevrejeva, S.: Application of the cross wavelet transform and wavelet coherence to geophysical time series, Nonlin. Processes Geophys., 11, 561–566, doi:10.5194/npg-11-561-2004, 2004.

Jayne, S. R. and Marotzke, J.: The dynamics of ocean heat transport variability, Rev. Geophys., 39, 385–411, 2001.

Johns, W. E., Baringer, M. O., Beal, L. M., Cunningham, S. A., Kanzow, T., Bryden, H. L., Hirschi, J. J.-M., Marotzke, J., Meinen, C. S., Shaw, B., and Curry, R.: Continuous, array-based estimates of Atlantic Ocean heat transport at 26.5° N, J. Climate, 24, 2429–2449, 2011.

Kanzow, T., Cunningham, S. A., Rayner, D., Hirschi, J. J.-M., Johns, W. E., Baringer, M. O., Bryden, H. L., Beal, L. M., Meinen, C. S., and Marotzke, J.: Observed flow compensation associated with the MOC at 26.5° N in the Atlantic, Science, 317, 938–941, 2007.

Kanzow, T., Johnson, H. L., Marshall, D. P., Cunningham, S. A., Hirschi, J. J.-M., Mujahid, A., Bryden, H. L., and Johns, W. E.: Basinwide Integrated Volume Transports in an Eddy-Filled Ocean, J. Phys. Oceanogr., 39, 3091–3110, 2009.

Kanzow, T., Cunningham, S. A., Johns, W. E., Hirschi, J. J.-M., Marotzke, J., Baringer, M. O., Meinen, C. S., Chidichimo, M. P., Atkinson, C., Beal, L. M., Bryden, H. L., and Collins, J.: Seasonal variability of the Atlantic meridional overturning circulation at 26.5° N, J. Climate, 23, 5678–5698, doi:10.1175/2010JCLI3389.1, 2010.

Killworth, P. D.: A simple linear model of the depth dependence of the wind-driven variability of the Meridional Overturning Circulation, J. Phys. Oceanogr., 38, 492–502, 2008.

Landerer, F. W., Wiese, D. N., Bentel, K., Boening, C., and Watkins, M. M.: North Atlantic meridional overturning circulation variations from GRACE ocean bottom pressure anomalies, Geophys. Res. Lett.,42, 8114–8121, doi:10.1002/2015GL065730, 2015.

Lin, Y., Greatbatch, R. J., and Sheng, J.: A model study of the vertically integrated transport variability through the Yucatan Channel: Role of Loop Current evolution and flow compensation around Cuba, J. Geophys. Res., 114, C08003, doi:10.1029/2008JC005199, 2009.

Longworth, H. R., Bryden, H. L., and Baringer, M. O.: Historical variability in Atlantic meridional baroclinic transport at 26.5° N from boundary dynamic height observations, Deep-Sea Res. Pt. II, 58, 1754–1767, 2011.

McCarthy, G., Frajka-Williams, E., Johns, W. E., Baringer, M. O., Meinen, C. S., Bryden, H. L., Rayner, D., Duchez, A., Roberts, C. D., and Cunningham, S. A.: Observed interannual variability of the Atlantic MOC at 26.5° N, Geophys. Res. Lett., 39, L19609, doi:10.1029/2012GL052933, 2012.

McCarthy, G. D., Smeed, D. A., Johns, W. E., Frajka-Williams, E., Moat, B. I., Rayner, D., Baringer, M. O., Meinen, C. S., and Bryden, H. L.: Measuring the Atlantic meridional overturning circulation at 26° N, Prog. Oceanogr., 130, 91–111, doi:10.1016/j.pocean.2014.10.006, 2015.

Meinen, C. S., Baringer, M. O., and Garcia, R. F.: Florida Current transport variability: An analysis of annual and longer-period signals, Deep-Sea Res. Pt. I, 57, 835–846, 2010.

Mielke, C., Frajka-Williams, E., and Baehr, J.: Observed and simulated variability of the AMOC at 26° N and 41° N, Geophys. Res. Lett., 40, 1159–1164, doi:10.1002/grl.50233, 2013.

Percival, D. B. and Walden, A. T.: Spectral Analysis for Physical Applications, Cambridge University Press, Cambridge, UK, 1998.

Pillar, H., Heimbach, P., Johnson, H., and Marshall, D.: Dynamical attribution of recent variability in Atlantic overturning, J. Clim, doi:10.1175/JCLI-D-15-0727.1, 2016.

Polo, I., Robson, J., Sutton, R., and Bamaseda, M.: The importance of wind and buoyancy forcing of the boundary density variations and the geostrophic component of the AMOC at 26° N, J. Phys. Oceanogr., 44, 2387–2408, 2014.

Rayner, D., Hirschi, J. J.-M., Kanzow, T., Johns, W. E., Wright, P. G., Frajka-Williams, E., Bryden, H. L., Meinen, C. S., Baringer, M. O., Marotzke, J., Beal, L. M., and Cunningham, S. A.: Monitoring the Atlantic meridional overturning circulation, Deep-Sea Res. Pt. II, 58, 1744–1753, doi:10.1016/j.dsr2.2010.10.056, 2011.

Roberts, C. D., Waters, J., Peterson, K. A., Palmer, M., McCarthy, G. D., Frajka-Williams, E., Haines, K., Lea, D. J., Martin, M. J., Storkey, D., Blockley, E. W., and Zuo, H.: Atmosphere drives observed interannual variability of the Atlantic meridional overturning circulation at 26.5° N, Geophys. Res. Lett., 40, 5164–5170, doi:10.1002/grl.50930, 2013.

Roberts, C. D., Jackson, L., and McNeall, D.: Is the 2004–2012 reduction of the Atlantic meridional overturning circulation significant?, Geophys. Res. Lett., 41, 3204–3210, doi:10.1002/2014GL059473, 2014.

Robson, J., Hodson, D., Hawkins, E., and Sutton, R.: Atlantic overturning in decline?, Nat. Geosci., 7, 2–3, doi:10.1038/ngeo2050, 2014.

Rousset, C. and Beal, L. M.: Closing the transport budget of the Florida Straits, Geophys. Res. Lett., 41, 2460–2466, doi:10.1002/2014GL059498, 2014.

Smeed, D. A., McCarthy, G. D., Cunningham, S. A., Frajka-Williams, E., Rayner, D., Johns, W. E., Meinen, C. S., Baringer, M. O., Moat, B. I., Duchez, A., and Bryden, H. L.: Observed decline of the Atlantic meridional overturning circulation 2004–2012, Ocean Sci., 10, 29–38, doi:10.5194/os-10-29-2014, 2014.

Smeed, D. A., McCarthy, G., Rayner, D., Moat, B. I., Johns, W. E., Baringer, M. O., and Meinen, C. S.: Atlantic meridional overturning circulation observed by the RAPID-MOCHA-WBTS (RAPID-Meridional Overturning Circulation and Heatflux Array-Western Boundary Time Series) array at 26° N from 2004 to 2014, available at: https://www.bodc.ac.uk/data/published_data_library/catalogue/10.5285/1a774e53-7383-2e9a-e053-6c86abc0d8c7/, last access: 15 August 2015.

Thomas, M. D. and Zhai, X.: Eddy-induced variability of the meridional overturning circulation in a model of the North Atlantic, Geophys. Res. Lett., 40, 2742–2747, doi:10.1002/grl.50532, 2013.

Wunsch, C.: Mass and volume transport variability in an eddy-filled ocean, Nat. Geosci., 1, 165–168, doi:10.1038/ngeo126, 2008.

Wunsch, C. and Heimbach, P.: Two decades of the Atlantic meridional overturning circulation: Anatomy, variations, extremes, prediction, and overcoming its limitations, J. Climate, 26, 7167–7186, doi:10.1175/JCLI-D-12-00478.1, 2013.

Xu, X., Chassignet, E. P., Johns, W. E., Schmitz Jr., W. J., and Metzger, E. J.: Intraseasonal to interannual variability of the Atlantic meridional overturning circulation from eddy-resolving simulations and observations, J. Geophys. Res., 119, 5140–5159, doi:10.1002/2014JC009994, 2014.

Yang, J.: Local and remote wind stress forcing of the seasonal variability of the Atlantic Meridional Overturning Circulation (AMOC) transport at 26.5° N, J. Geophys. Res., 120, 2488–2503, doi:10.1002/2014JC010317, 2015.

Yeager, S.: Topographic coupling of the Atlantic overturning and gyre circulations, J. Phys. Oceanogr., 45, 1258–1284, doi:10.1175/JPO-D-14-0100.1, 2015.

Zhao, J. and Johns, W.: Wind-forced interannual variability of the Atlantic Meridional Overturning Circulation at 26.5° N, J. Geophys. Res., 119, 2403–2419, doi:10.1002/2013JC009407, 2014.

Table 1. Mean $\pm$ standard deviation of transports for the first five years and latter five years, where years run from 1 April–31 March. Standard deviations are calculated on the annual averages. Statistically significant changes to the mean are indicated by bold, based on two-tailed t tests.

Component	2004–2009 [Sv]	2009–2014 [Sv]	Change [Sv]
FC	31.7 ± 0.2	31.0 ± 0.3	$\mathbf{-0.7}$
Ekman	3.7 ± 0.4	3.4 ± 1.0	-0.3
UMO	-17.0 ± 1.2	-18.8 ± 1.0	$\mathbf{-1.9}$
MOC	18.4 ± 1.3	15.5 ± 1.9	$\mathbf{-2.9}$
UNADW	-12.0 ± 0.3	-11.8 ± 0.7	0.2
LNADW	-7.1 ± 0.9	-4.7 ± 1.5	**2.3**

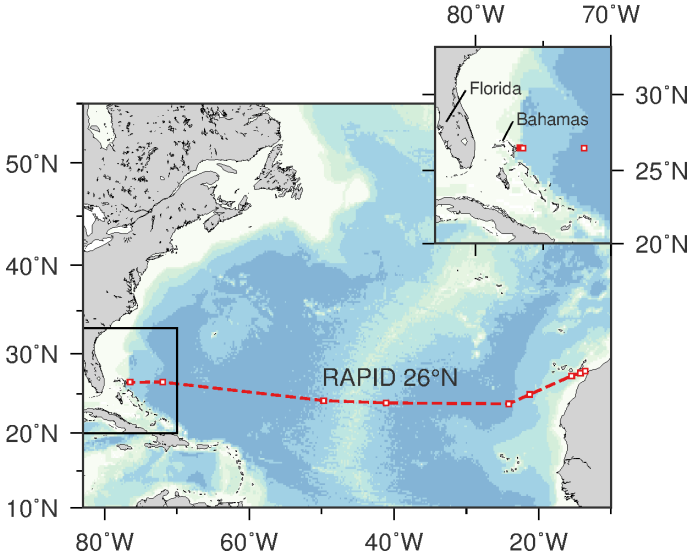

Figure 1. Map of the study area. The RAPID array is shown with dashed lines crossing the Atlantic around 26°N. Mooring positions are given by red squares. The inset is marked by the black rectangle, and shows a zoomed in view of the western boundary region.

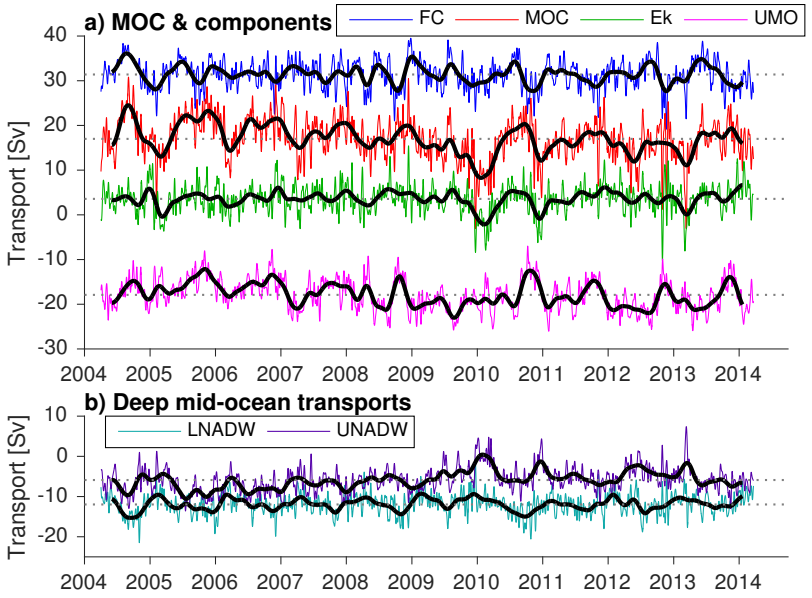

Figure 2. (a) Transport time series of the FC (blue), Ekman (green), upper mid-ocean (magenta) and overturning (red) at ten-day resolution. **(b)** Layer transports for UNADW (1100–3000 m, cyan) and LNADW (3000–5000 m, purple). For visualization purposes, the filtered versions of the time series are shown in black, where transports have been convolved with a 4-month, low-pass Hanning window. Transports are positive northwards. Ten-year mean transports for each components are shown with the dotted lines.

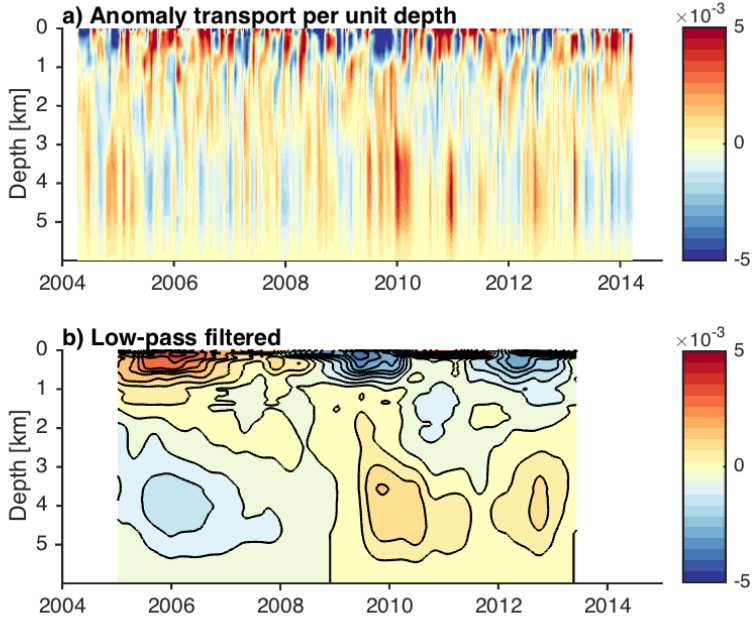

Figure 3. Transport-per-unit-depth anomalies of the mid-ocean transport at 26° N, where the time mean profile over the ten years has been removed. **(a)** The top panel shows the twice-monthly, deseasonalized variability and **(b)** the lower panel is further filtered with the 1.5 year filter. Red (blue) shows transports which are anomalously northward (southward).

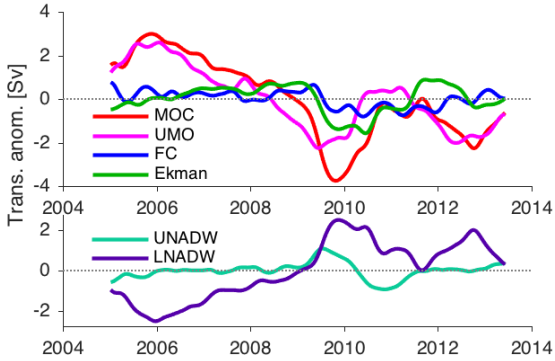

Figure 4. Time series of transport anomaly for MOC and components as in Fig. 2, deseasonalized and low-pass filtered with 1.5 year filter.

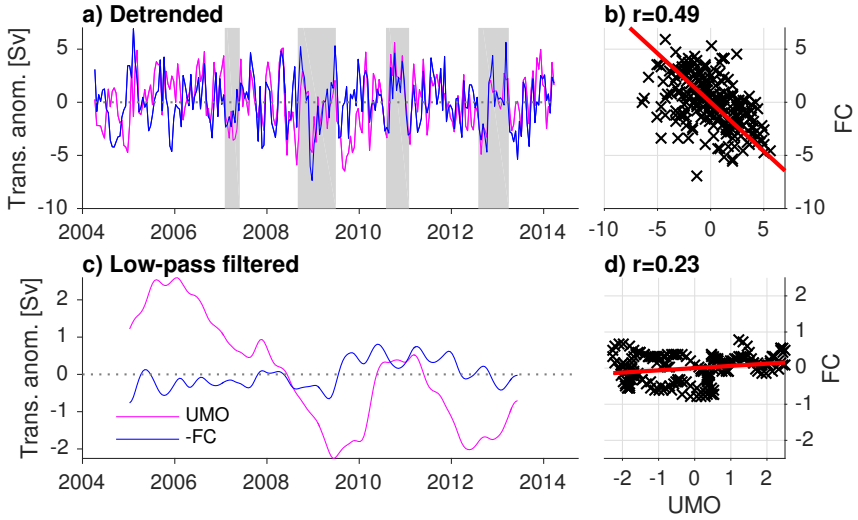

Figure 5. Transport anomaly time series (left column) for the −FC (blue) and UMO (magenta). Zero anomaly is marked with the dashed line. Scatter plots of the same (right column) with correlation coefficients (r) noted. In **(a, b)**, the deseasonalized, detrended time series are used. In **(c, d)**, the time series are deseasonalized and low-pass filtered, but not detrended. The orthogonal regression line is overlaid on the scatter plots. Grey bars highlight periods noted in the text.

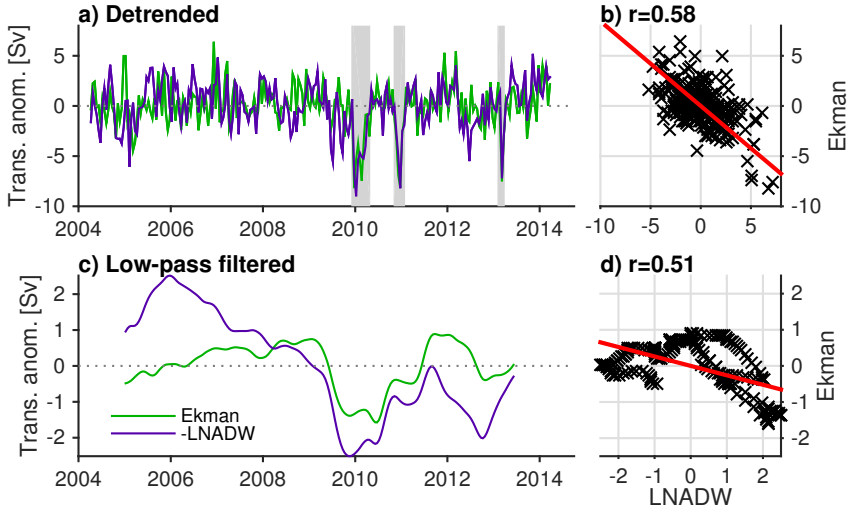

Figure 6. As Fig. 5 but for the Ekman and −LNADW transport anomaly time series.

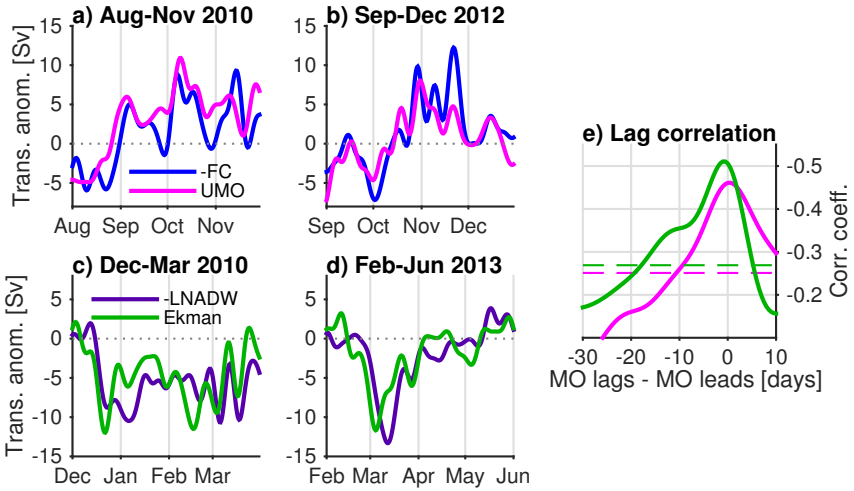

Figure 7. Ten-day filtered transport anomaly time series of UMO and FC **(a, b)** and LNADW and Ekman **(c, d)**. The ten-year mean has been removed, but the seasonal cycle and trends are retained. Time ranges have been chosen to correspond to large anomalies in both time series, to visualize possible lags. **(e)** Lag correlation between ten-day filtered UMO and FC (magenta) and Ekman and LNADW (green). 95 % significance is marked by the dashed lines, same color.

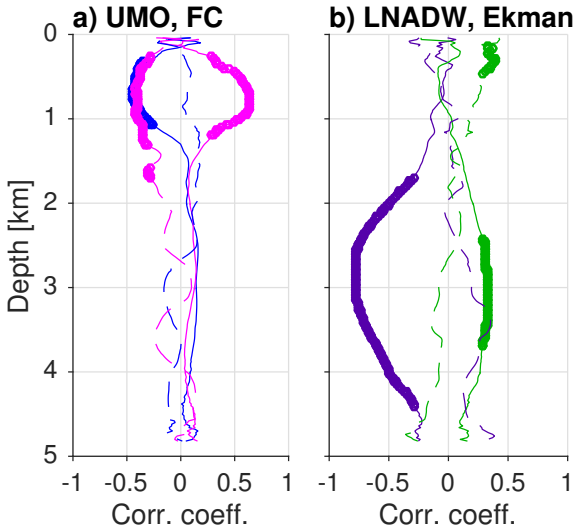

Figure 8. Correlation between isopycnal displacements at each depth and transport time series, where time series are deseasonalized and detrended. **(a)** Correlation between UMO (magenta) and isopycnal displacements at the west (solid) and east (dashed), and between FC (blue) and isopycnal displacements at the west (solid) and east (dashed). Significant correlations are indicated by the thicker line. **(b)** The same, but for LNADW (purple) and Ekman (green).

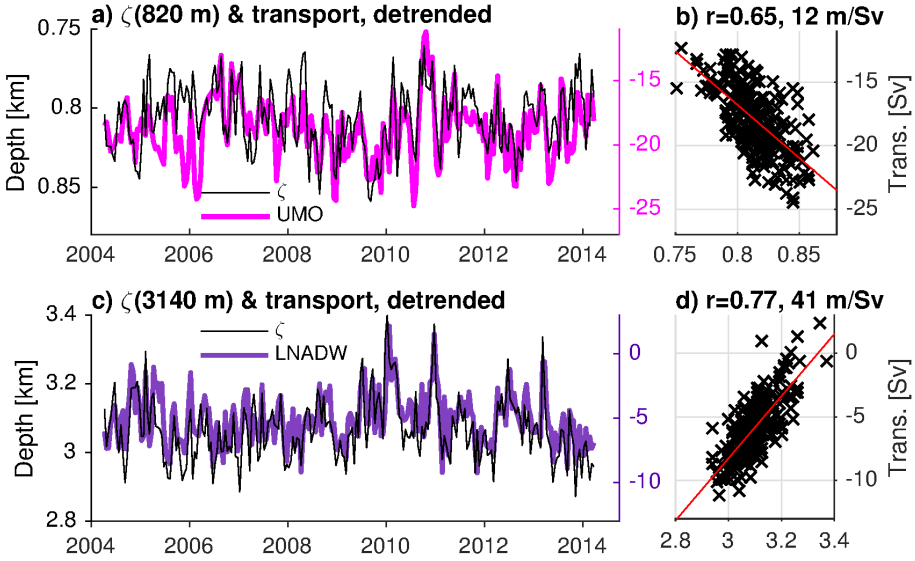

Figure 9. Time series of deseasonalized, detrended transports and isopycnal depths. **(a)** UMO transport (magenta) and the depth of the density surface with mean position at 820 m (highest correlation with UMO) at the west. **(c)** LNADW transport (purple) and the depth of the density surface with highest correlation (at 3140 m). Scatter plots are shown in **(b, d)**, where the least squares linear regression is overlaid.

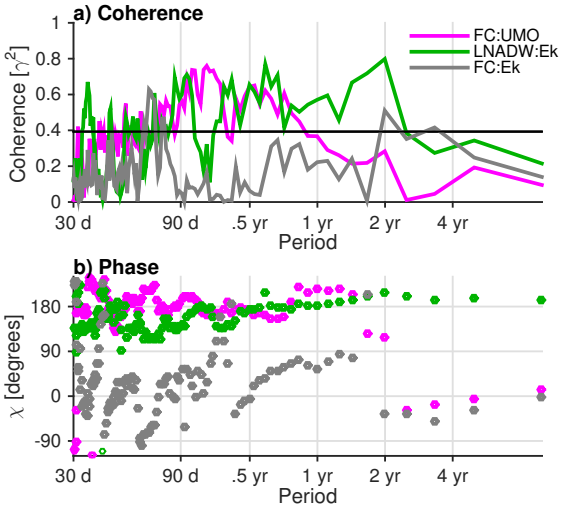

Figure 10. Coherence between MOC components: UMO and FC (magenta), LNADW and Ekman (green) and FC and Ekman (grey), where time series are the original 10 day filtered (seasonal variations retained). The top panel shows coherence, where significance is delimited by the black horizontal line. The lower panel shows the phase relationship at each period in degrees.

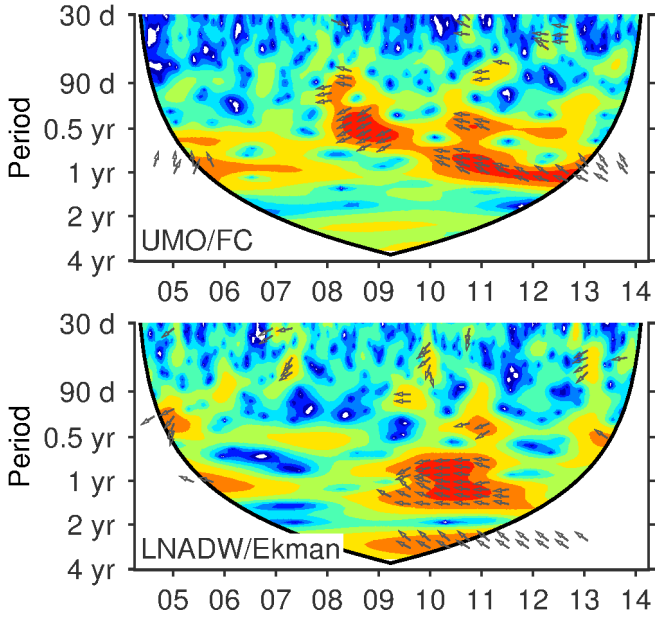

Figure 11. (a) Cross wavelet transform between the FC and UMO shows high power (red) with a fixed phase-relationship since 2007 at periods between 60–400 days. **(b)** Cross wavelet transform between Ekman and LNADW shows high power primarily at annual periods during the 2009–2010 events, as well as sub-annual from 50–150 days in 2005, 2011, and 2013 (Arrows pointing to the left indicate out-of-phase relationship or anti-correlation, and are only shown when the relationship is significant. Deviations from 180 ° indicate a lag or phase shift.).

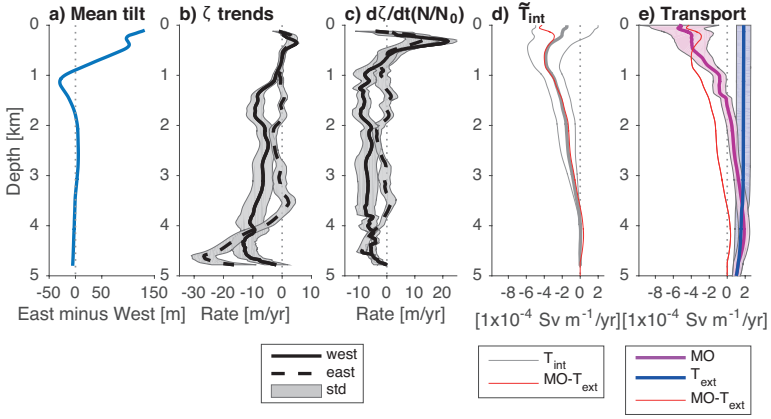

Figure 12. Trend in isopycnal displacements and transports. **(a)** Mean height difference between isopycnals in the east and west. **(b)** Trend in isopycnal displacements at the western and eastern boundaries, where a negative (positive) trend indicates downward (upward) movement of isopycnals. The solid (dashed) line is for displacements at the west (east). **(c)** Trend in displacements scaled by buoyancy frequency with $N_0 = 1 \times 10^{-3}\,\mathrm{s}^{-1}$. **(d)** Trend in $\widetilde{T}_{\mathrm{int}}$ from Eq. (2). The red line is the trend in $\mathrm{MO}(z) - T_{\mathrm{ext}}$. **(e)** Trends in transport-per-unit-depth of mid-ocean ($\mathrm{MO}(z)$) in magenta, T_{ext} in blue. All time series were twice-monthly. Confidence intervals on the trends are shaded. The dotted line shows a zero trend.